Scanning Microscopy Vol. 11, 1997 (Pages 155-169) 0891-7035/97$5.00+.25
Scanning Microscopy International, Chicago (AMF O'Hare), IL 60666 USA

THE MOVING WINDOW SHANNON RECONSTRUCTION (MWSR) IN REAL AND FOURIER DOMAIN AND ITS USE IN TOMOGRAPHY

S. Lanzavecchia* and P.L. Bellon

Dipartimento di Chimica Strutturale e Stereochimica Inorganica, Università degli Studi, Milano, Italy

Abstract

The article illustrates the interpolation techniques based on the "moving window Shannon reconstruction" (MWSR) and demonstrates its performance in real and Fourier domain. Interpolation in reciprocal domain is relevant to tomographic reconstructions *via* direct Fourier methods (DFM). With these techniques, a structure is reconstructed by interpolating its FT coefficients in Cartesian coordinates from the transforms of projections, and by inverting the result to real space. Although the samples are not equally spaced according to Euclidean metric, the MWSR can be used provided that an invertible transformation exists which maps the sampling points in a new coordinate system in which they are evenly distributed. These coordinate transformations are illustrated for the polar geometry of X-ray tomography and for electron tomography with random conical tilt. DFM and convoluted back-projection are compared on the basis of quantitative parameters.

Key Words: Shannon reconstruction, Shannon reconstruction moving window, tomography, direct Fourier methods in tomography, X-ray computer tomography, electron tomography.

*Address for correspondence:
S. Lanzavecchia
Dipartimento di Chimica Strutturale
Università degli Studi
via Venezian 21, 20133 Milano, Italy
Telephone number : +39-02-2361410
FAX number : +39-02-70635288
E-mail: salvator@csmtbo.mi.cnr.it

Introduction

In signal and image processing as well as in tomography and in many other computer-based sciences, functions which are assumed to be continuous are measured and stored in a sampled form. Thus, numeric elaborations deal with huge arrays of numbers spanning one- or multi-dimensional spaces. An ubiquitous task consists of retrieving the value of a function in points that have not been actually measured. Apart from special circumstances, this problem cannot be solved exactly: "it is just this arbitrary division of continuum into discontinuous units that gives rise to a large proportion of errors" (L. Tolstoj, *War and Peace*, III, 3, 1).

The process of retrieving unknown values from known ones is called interpolation or resampling or even "reconstruction" (e.g., Wolberg, 1990), though scientists working in tomography would prefer the latter term to be reserved for the process of obtaining a function from its projections. A number of algorithms can be used to accomplish the task; the accuracy of the retrieved values depends on the algorithm used, on the type function involved and on the layout of samples.

Available methods belong to two main classes, based either on polynomials or on harmonic functions. The first class adopts spline-type functions (Hou and Andrews, 1978) and comprises the nearest-neighbor approximation and the linear interpolation which may be considered as a zero- and first order splines. A spline interpolation is based on the Taylor series expansion (e.g., Unser *et al*., 1995) and the function recovered is a piece wise polynomial, continuous with continuous derivatives up to the spline order. Fractional errors are proportional to d^n, where d is the distance from the nearest original sample and n the spline order. One important advantage of splines is that the function does not need to be sampled with constant rate and this makes it possible to obtain an even distribution from uneven spaced samples (e.g., Tosoni *et al*., 1995).

Interpolation with harmonic functions is based on the sampling theorem (Shannon, 1949) and is often referred to as "Shannon reconstruction". In theory, under a number of assumptions, this technique is able to recover *exactly* the function from equally spaced samples. In spite of this

attractive property, a rigorous Shannon reconstruction is never performed, even for one-dimensional (1D) functions, because of its prohibitive computation cost. However, interpolations with high-order splines may also be difficult to implement and time consuming.

We have recently introduced some innovations in the Shannon reconstruction, in an algorithm that we call "moving window Shannon reconstruction" (MWSR). The method is suitable for the case of functions sampled with constant rate and yields outstanding results as far as accuracy is concerned. (Lanzavecchia and Bellon, 1994, 1995). In this paper we shall briefly introduce the Shannon theorem, its application to finite intervals, and the MWSR. Subsequently, we will illustrate some results, obtained in real domain, in removing the relative distortions from equivalent images or cell sections. In our implementation of distortion removal, interpolation is used iteratively on the same image; the process is shortly discussed here to show that a function can be resampled a number of times with MWSR without significant loss of power up to a predetermined frequency. Concerning tomography, we will illustrate and discuss the use of MWSR in "Direct Fourier Methods" (DFM) of reconstruction. A DFM consists of recovering the *n*-dimensional Fourier transform (FT) of a function from (*n*-1)-dimensional FT of its projections. The latter provide a sampling of the function FT in a given coordinate system which is to be converted into Cartesian coordinates. Resampling in Fourier space is often regarded as a cumbersome task, both because of the peculiarity of data in the frequency domain and of the layout of samples (Lewitt, 1983). Actually, conversion from a system of coordinates to another in the Fourier domain is the crux of DFM, though the inherent accuracy of MWSR can overcome all problems and yield extremely accurate results.

The Shannon Reconstruction

According to Shannon's theorem, a band-limited function *f* can be exactly reconstructed in its continuous domain from an *infinite* number of discrete samples, equally spaced. If ω_c is the maximum frequency component of *f*, the distance δ between the samples must satisfy the condition: $\delta \leq \pi/\omega_c$. According to this hypothesis, the reconstruction equation is:

$$f(x) = \sum_{j=-\infty}^{+\infty} f(j \bullet \delta) \frac{\sin\left[\pi \bullet \left(\frac{x}{\delta} - j\right)\right]}{\pi \bullet \left(\frac{x}{\delta} - j\right)} \qquad (1)$$

The value ω_c/π is called the Nyquist sampling rate, and is just below the minimum rate required to detect the component ω_c. Equation (1) represents a discrete convolution between *f* and an interpolating sinc kernel: sin $(\pi x)/\pi x$.

Equation (1) is of great theoretical importance but cannot be used as such. If the number of samples is finite, then the series is truncated. This is equivalent to assuming *f* to be zero out of the sampling interval, an assumption that contradicts the hypothesis: a space limited function cannot be band-limited, apart from the trivial case of $f = 0$.

The approximation introduced by the fact that the number of samples is finite can be eliminated if the function is considered to be periodic along the real axis, with a period equal to the sampling interval. This hypothesis is automatically implied in most Fourier analyses. Under this assumption and for an *odd* number of samples, a reconstruction function can be obtained with use of the "Fourier series kernel" (Papoulis, 1962):

$$\varphi(x) = \frac{1}{N} \sum_{j=0}^{N-1} f\left(\frac{j}{N}\right) \frac{\sin\left[N \bullet \pi \bullet \left(x - \frac{j}{N}\right)\right]}{\sin\left[\pi \bullet \left(x - \frac{j}{N}\right)\right]} \qquad (2)$$

As is true for Equation (1), this is a discrete convolution of the samples with an interpolating kernel. Papoulis (1966) has shown that, under certain hypotheses, a function can be reconstructed from its *N* samples by convolution with many different interpolating kernels. For an *even* number of samples, Yuen and Fraser (1979) have derived the following reconstruction equation:

$$\psi(x) = \frac{1}{N} \sum_{j=0}^{N-1} f\left(\frac{j}{N}\right) \frac{\sin\left[N \bullet \pi \bullet \left(x - \frac{j}{N}\right)\right]}{\tan\left[\pi \bullet \left(x - \frac{j}{N}\right)\right]} \qquad (3)$$

We have recently shown (Lanzavecchia and Bellon, 1995) that the reconstructing functions φ and ψ are members of a family:

$$\phi^A(x) = \frac{1}{N} \sum_{j=0}^{N-1} f\left(\frac{j}{N}\right) \frac{\sin\left[N \bullet \pi \bullet \left(x - \frac{j}{N}\right)\right]}{\sin\left[\pi \bullet \left(x - \frac{j}{N}\right)\right]} \bullet \left\{\cos\left[\pi \bullet \left(x - \frac{j}{N}\right)\right]\right\}^A \qquad (4)$$

where *A* is even for *N* odd and *vice versa*. Equations (2) and (3) correspond to ϕ^0 and ϕ^1 respectively. Some interpolating kernels k^A are drawn in Figure 1 for an interval with 32 samples.

Equation (4) applies rigorously only if *f* is a trigono-

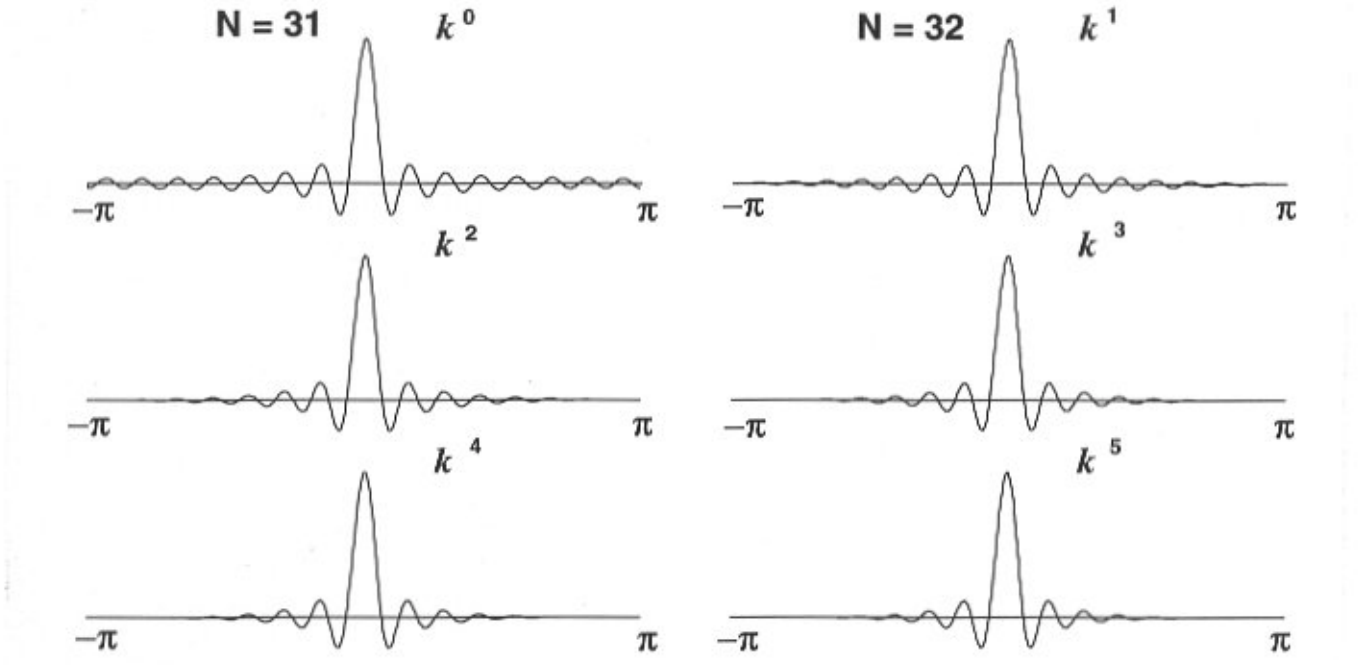

Figure 1. The shape of some interpolating kernels $k^A(x)=(\sin Nx/\sin x)(\cos x)^A$ in the period $[-\pi,\pi]$. Kernels with even and odd A are drawn for intervals sampled in 31 and 32 points, respectively.

metric polynomial whose finite degree is lower than the maximum observable frequency dictated by the sampling rate.

Since periodicity is assumed, the validity of this hypothesis depends upon *f*, and the choice of the sampling interval is important.

The conditions which fully justify the application of Equation (4) are seldom verified so that ϕ^A generally represents an approximation to *f*, though more correct than that obtained by truncating Equation (1). In any event, if *N* is large, convolutions of the type shown above require long computation times. If the summations of Equations (2) and (3) are drastically limited to a small window of samples around the point to be interpolated, the results are worse than those obtained with spline algorithms (Hou and Andrews, 1978) and this is true also with all kernels represented in Equation (4). Truncated reconstructions are inaccurate because the kernels keep oscillating even very far from the short window interval.

The Moving Window Shannon Reconstruction

Until now we have formulated a family of reconstruction equations which perform a discrete convolution of *all* samples with the interpolating kernel. The simple innovation of MWSR consists of regarding a small window of *n* points ($n<<N$), moving along the sampling interval, as an entire sampling interval in which the convolution is performed. The center of the window is positioned on the value to be resampled. Let an index *m* label the first sample within the window; *m* is displaced by about *n*/2 from the point to be reconstructed. With this notation the reconstruction equation becomes:

$$\phi_n^A(x)=\frac{1}{n}\sum_{j=m}^{m+n-1} f\left(\frac{j}{N}\right)\frac{\sin\left[\pi\bullet\left(x-\frac{j}{N}\right)\right]}{\sin\left[\frac{\pi}{n}\bullet\left(x-\frac{j}{N}\right)\right]}\bullet \left\{\cos\left[\frac{\pi}{n}\bullet\left(x-\frac{j}{N}\right)\right]\right\}^A \qquad (5)$$

The suffix *n* is now attached to ϕ to highlight the window width. In this way the number of convoluting coefficients can be lowered almost at wish, without truncation; the interpolating kernel is modified and adjusted to match the width of the moving window.

Assuming the window to be a complete sampling interval is equivalent to saying that the function is periodic with a period equal to the moving window. Thus, ϕ_n^A is equal to *f* only if the latter is a finite trigonometric polynomial in every sub-interval of width *n*, a condition which is seldom fulfilled. This rough approximation is the source of errors,

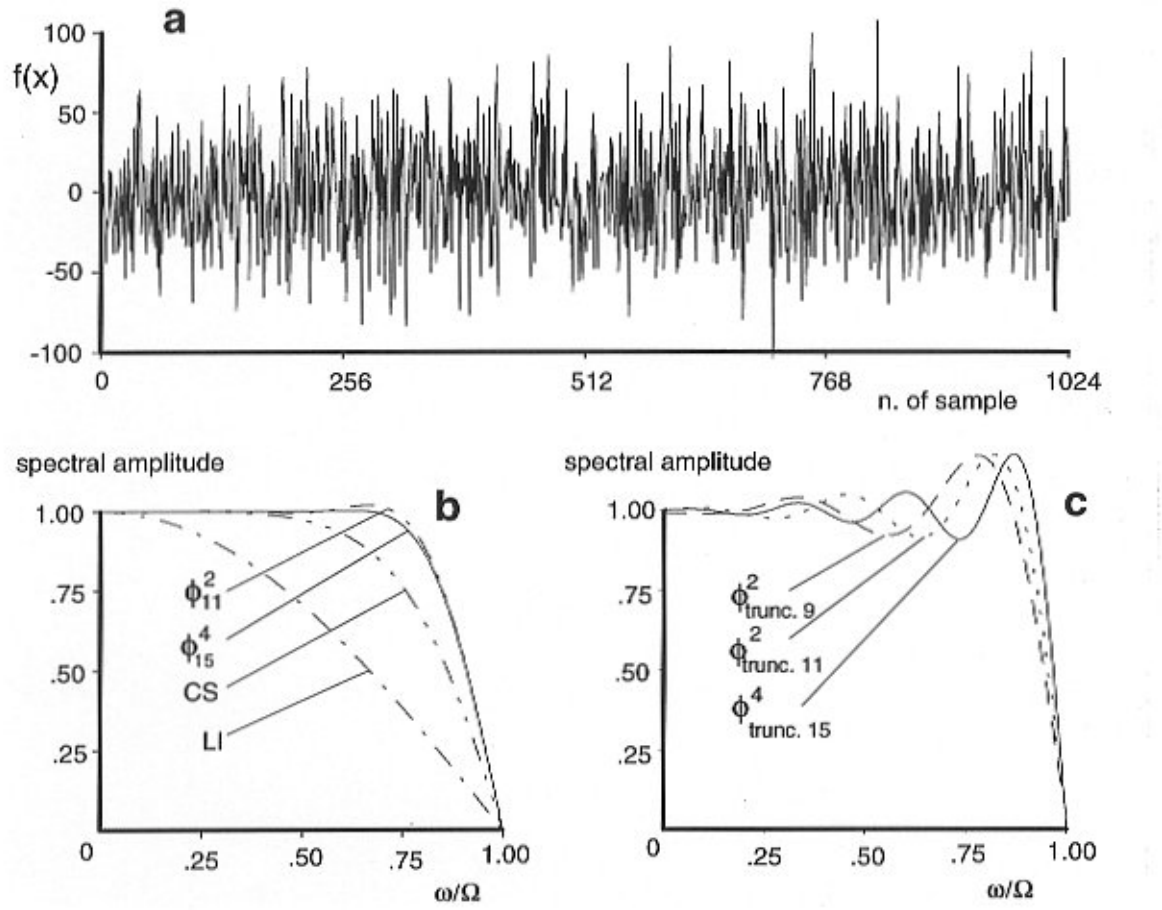

Figure 2. The test function shown in (**a**), sampled in 1024 points, is obtained by inverting a FT with unit moduli and random phases up to the maximum observable frequency (511); (**b**) amplitude spectra of the test signal shifted by half a sample with MWSR and two different kernels, with linear interpolation (LI) and cubic spline (CS); (**c**) same results with the Shannon reconstruction of Equation (4), truncated to 9, 11 and 15 samples.

because of the spectral aliasing originating from the discontinuities at the opposite borders of the window. In this connection, the shape of the kernel, whose period matches the width of the window, becomes important. As *A* increases, the kernels of Equation (4) strongly dampen near the borders of the window as shown in Figure 1. Kernels with severe dampen underweight the samples at the borders and limit the presence of *alias* components.

The performance of the MWSR can be quantitatively assessed either in Fourier or in real domain. In the former case, all samples of a function with a known spectral response are shifted by a fractional amount and the shift-independent spectrum is compared with the original. For a comparison in real domain it is convenient to shift the function twice, back and forth, so that the result is directly comparable with the original. Functions appropriate for these tests can be obtained by inverting 1D transforms with all moduli set to one, up to a prescribed frequency, and setting phases at random. One of them, computed on 1024 samples with unit moduli up to the Nyquist frequency (511) is shown in Figure 2a; though reminiscent of white noise, this function has a period matching the sampling interval and wraparound properties so that a Shannon reconstruction based on all samples would reconstruct the function exactly whereas a MWSR does so only approximately. The shift test based on the spectral response has been performed by interpolating the function at every middle points between two original samples and by computing the spectrum of the result. If the resampling is repeated in the opposite direction, then the final array becomes comparable with the original one in the real domain. Spectral comparisons are reported in Figures 2b and 2c and errors are shown in Table 1 for different functions and different kernels.

Switching from 1D to two-dimensional (2D) interpolation, a 2D implementation of Equation (5) is straightforward:

Table 1. Maximum absolute error (MAE) and root mean square deviation (rmsd) in % of the dynamic range, obtained in a double shift (forth and back by half a sample) of the function of Figure 2a. Shifts are performed with interpolations based on a truncation of Equation (4), on the MWSR and different kernels, or on cubic spline (CS) and linear interpolation (LI).

algorithm	Maximum component frequency (1024 samples)			
	384 (75 %)		256 (50 %)	
	MAE	rmsd	MAE	rmsd
$\varphi^2_{\text{trunc. 9}}$	9.1	2.4	5.3	1.7
φ^2_9	1.9	0.6	0.3	0.1
$\varphi^2_{\text{trunc.11}}$	5.3	1.8	4.7	1.6
φ^2_{11}	0.8	0.3	0.2	0.1
$\varphi^4_{\text{trunc.15}}$	5.0	1.5	3.8	1.1
φ^4_{15}	0.8	0.2	0.03	0.02
C.S.	6.7	2.2	0.9	0.3
L.I.	25.3	7.6	14.1	3.8

$$\phi_n^A(x,y) = \frac{1}{n^2} \sum_{j=m}^{m+n-1} \sum_{i=\ell}^{\ell+n-1} f(j,i) \frac{\sin[\pi(x-j)]}{\sin\left[\frac{\pi}{n}(x-j)\right]} \bullet \frac{\sin[\pi(y-i)]}{\sin\left[\frac{\pi}{n}(y-i)\right]} \left\{\cos\left[\frac{\pi}{n}(x-j)\right]\right\}^A \left\{\cos\left[\frac{\pi}{n}(y-i)\right]\right\}^A \quad (6)$$

The time spent in computing transcendental coefficients might be prohibitive, even with small windows. In our implementations of the MWSR, the coefficients are stored in a look-up table (Lanzavecchia and Bellon, 1994). The window of n^2 samples used in Equation (6) requires two sets of n different values. Each set depends upon the distance of the x or y coordinate from the left nearest j or from the bottom nearest i indices. These fractional distances, multiplied by the number of pages of the table and converted to integers, address the positions in which the two sets are stored.

Applications to Real Domain

Electron tomography with single axis tilting frequently deals with 2D crystalline arrays. The large number of repeating units contained within a single micrograph is the key for low-dose, high resolution studies of macromolecular assemblies (e.g., Henderson *et al.*, 1990; Jap *et al.*, 1991). This resolution is achieved by combined use of images and electron diffraction patterns and of techniques designed to suppress crystal disorder (Henderson *et al.*, 1986). The refinement of strategies to detect and remove lattice distortion seems to be continuing (Saxton *et al.*, 1992). Crystal imperfections are detected and resampling schemes are adopted to obtain regular crystal portions, suitable for spectral analysis and tomography. Most often, sophisticated unwarping approaches are based on linear interpolation.

The problem of warping is encountered in morphological studies of large and complex organelles such as flagella and cilia. These can be sectioned and portrayed in the electron microscope (EM) to obtain sets of equivalent images, though distorted with respect to each other. If distortions are removed, then a number of sections can be averaged to get "restored" images with improved signal-to-noise (S/N) ratio (Bellon and Lanzavecchia, 1992). To accomplish this, images with different ellipticity are stretched to a circular shape and rotated; at this point relative distortions can be detected and eliminated by further resampling steps. Certain sections show arrays of organelles or parts of them (e.g., Lanzavecchia *et al.*, 1991) which, in spite of an evident crystalline order, are distorted to such an extent that restoring them by filtration of non-periodic components would make no sense. With large and complex structures, such as flagellar doublets or entire axonemes, the process of removing distortions to finer and finer levels may require 4 or 5 iterations. Suppose that this iterated process is done with linear interpolation which, in 1D resampling, cuts 10% of the amplitude of spectral components at about 0.3 times the maximum frequency. After n 2D interpolations those amplitudes will be reduced by a factor of 0.9^{2n}. Iterated resampling without power loss is possible if the interpolation algorithm ensures the preservation of all spectral amplitudes up to the highest significant component of the pattern. In the first attempts to improve the results of Fourier filtering of biological 2D crystals by resampling (Crowther and Sleytr, 1977), the authors were disappointed by the lack of significant band-pass improvement. Most probably, linear interpolation was the reason for such unsatisfactory results.

We have shown (Bellon and Lanzavecchia, 1992) that it is possible to iterate quite a few resampling steps in distorted crystalline arrays using the MWSR. The improvement obtained can be appreciated by comparing

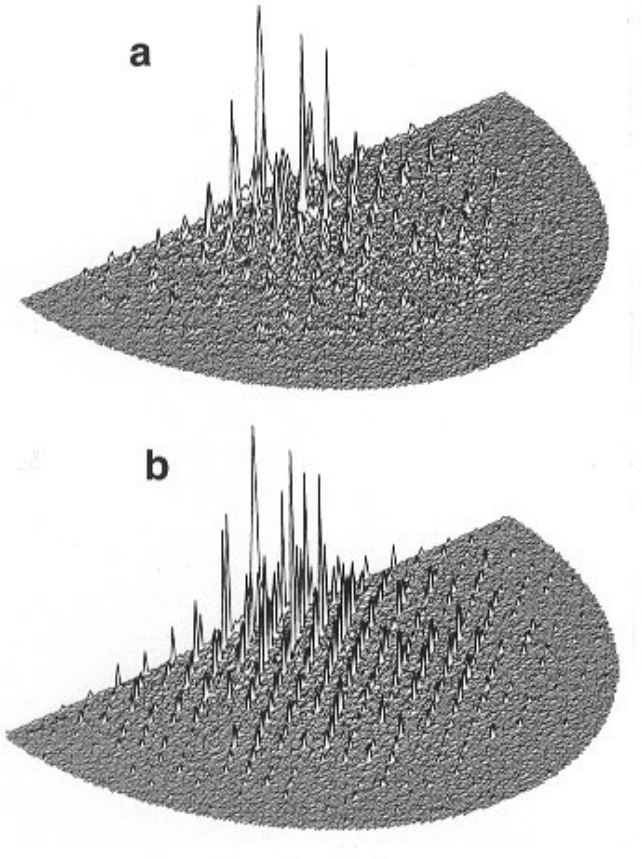

Figure 3. Amplitude spectra of a periodic array of cilia (section of a *Ctenophore* macrocilium), before and after distortion removal. In spite of remarkable periodicity, the 2D crystal is distorted as evidenced by the severe broadening of spectrum (**a**). The spectrum shown in (**b**) is obtained with four iterations of a process of distortion removal. Peaks are much sharper and high frequency components, not observable in (a), are well preserved in the resampling iterations.

---

the two amplitude spectra of Figures 3a and 3b. The pattern analyzed, not shown here, was a section of a macro-cilium of a *Ctenophore* with a cell edge of about 300 nm. The spectrum in Figure 3b, not filtered, was obtained after a four-fold resampling. The comparison of the two spectra explain why we call this iterated resampling a "power harvesting" algorithm.

Non Euclidean sampling

We have already shown in Equation (1) how a band limited function *f(x)* can be recovered from a set of evenly spaced samples $\{x_j=j\delta\}$. Consider now a set of not equally spaced samples $\{x_j\}$; according to Clark *et al*. (1985), if a transformation $\gamma(x) = \tau$ exists, such that $\gamma(x_j)=j\delta$, a new function $h(\tau)=h(\gamma(x)) \equiv f(x)$ is available. The function h comes out to be evenly sampled in τ, since $h(j\delta)=f(x_j)$; if $h(\tau)$ is band-limited, Equation (1) can be applied to reconstruct it, and therefore to reconstruct f:

$$f(x) \equiv h(\gamma(x)) = \sum_{j=-\infty}^{+\infty} f(x_j) \frac{\sin\left[\pi \bullet \left(\frac{\gamma(x)}{\delta} - j\right)\right]}{\pi \bullet \left(\frac{\gamma(x)}{\delta} - j\right)} \qquad (7)$$

The conditions which make the reconstruction of Equation (7) exact are discussed in the paper by Clark *et al*. (1985); briefly, both f and h should be band-limited and an invertible transformation should exist. If this is not strictly valid, Equation (7) represents only an approximation. In the same way as Equation (7) is derived from Equation (1), the equivalent of Equations (2)-(5) may be obtained. If the MWSR is adopted, then the damping of the kernel is useful to reduce aliasing effects. It should be noted that the argument of the kernel in Equation (7) depends upon $\gamma(x)$ rather than upon x; this implies that the distance between the point to be reconstructed and the original samples of f is to be measured according to a metric corrected by the transformation. These distances are usually different with respect to the metric of the original space.

A polar raster is a typical sampling grid in which the points are lying at uneven Euclidean intervals, though equally spaced in r and θ. The transformation of coordinates from Cartesian to polar is the invertible mapping which connects the two samplings.

The MWSR in DFM Tomographic Reconstructions

A function can be reconstructed from projections provided that their number is high enough and that the projecting directions are well distributed (e.g., Hoppe and Hegerl, 1980; Radermacher, 1988). This distribution of projecting directions has a counterpart in reciprocal space, since the FTs of projections are central sections of the function transform. In three dimensions, the transform of the function to be reconstructed is sampled by a set of 2D transforms and this offers the possibility to resample the overall transform in Cartesian coordinates and to obtain the reconstruction by a simple Fourier inversion. This kind of process is called a "direct Fourier method" (DFM).

With regard to resampling, reciprocal space is perfectly equivalent to direct space. The Fourier transform operator maps functions from $L^2(\Re)$ to $L^2(\Re)$, so that both the original function and its transform belong the same Hilbert space (Plancharel theorem, see, e.g., Rudin, 1974). Thus, the Shannon criterion, valid in real domain, applies to reciprocal domain as well. Furthermore, for a function with finite support, the relationship between the discrete Fourier series, computed with respect to the support, and the

continuous transform is such that the coefficients of the former represent a discrete sampling of the latter (Brigham, 1974). In order to use the Shannon reconstruction, the band extension of the transform must be finite; a difficulty might arise in the correct evaluation of this extension.

The Radon theorem requires the projections to be collected from an isolated object, that is, from a function with compact support. This hypothesis agrees with the idea of sampling the overall transform of the object by central sections, that is, by the discrete transforms of finite projections. Clearly, the tomographic reconstruction is exact if the type of sampling in Fourier space is adequate to the band-pass of the FT of the object, i.e., if it satisfies the Shannon criterion.

DFM in X-ray CT

All clinical imagery produced by X-ray CT is obtained with convoluted back-projection methods (CBPM), though DFM algorithms have been suggested (Stark *et al*., 1981; Peng and Stark, 1987; Matej and Bajla, 1990). Clinical X-ray CT is a 2D problem in which the transforms of 1D projections represent a polar sampling of the 2D FT to be recovered and inverted. The resampling performed in a DFM is therefore a conversion from polar to Cartesian coordinates.

X-ray scanners use a fan-beam geometry because the photons impinging on the array of detectors come from a point source. Thus, two distinct resampling processes are needed. In a first step (the *rebinning)* experimental data are converted by interpolation to the parallel geometry of Radon transform (Rosenfeld and Kak, 1982). In the second, the conversion of coordinates is carried out. Since X-ray CT reconstructions require high resolution and quantitative attenuation data, the finite width of counters has to be taken into account (Bellon and Lanzavecchia, 1997). Kernels to deconvolute this effect are designed on the basis of the resolution required and of the particular tissue to be examined. We have shown elsewhere that DFM reconstructions with use of the MWSR in both resampling steps are perfectly equivalent to those obtained by CBPM on clinical instruments (Bellon and Lanzavecchia, 1995). Figure 4 shows the same high-resolution detail of inner ear bones, obtained by DFM and CBPM; as one can see, the two images are indistinguishable.

It is worth mentioning that, on a modern workstation, the reconstruction of a X-ray CT slice with DFM runs 35-55 times faster than with CBPM. In electron tomography, an equivalent DFM can be used to reconstruct all slices orthogonal to the rotation axis in single axis tilting geometry (Lanzavecchia *et al*., 1993).

Electron tomography with random conical tilt.

Random conical tilt is an elegant method of electron tomography which allows different projections of a macromolecular assembly to be collected with minimum radiation damage (Radermacher *et al*., 1987). The random aspect of the method arises from the fact that the azimuthal angles ϕ of projections may assume any value. Since, however, there is a resolution limit in their evaluation, these angles can be assumed to represent a set of discrete values, separated by a constant amount in the interval $[0, 2\pi)$; the

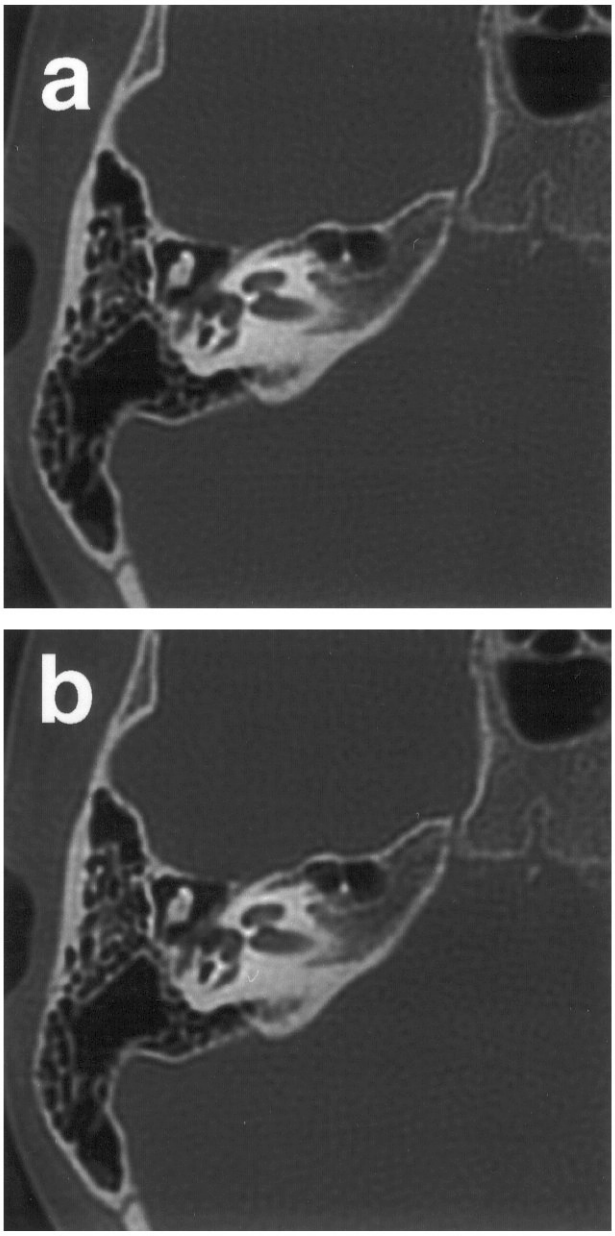

Figure 4. X-ray CT reconstructions of inner ear bones. No differences are noticeable among image (**a**) (convoluted back projection done by a clinical instrument) and image (**b**) (direct Fourier method with MWSR).

error can be thought of as an azimuthal jitter with maximum extent of $\Delta\phi/2$. Based on this assumption, we have proposed a DFM approach which uses the MWSR (Lanzavecchia *et al.*, 1993). The method, embedded in a package called "SPAtial Reconstruction Kernel" (SPARK), consists of recovering the 3D FT in Cartesian coordinates from a set of planar transforms (2D FT of projections) which are sampling the reciprocal space as shown in Figure 5a.

The coefficients coming from 2D FT of all projections lie on a set of coronas, one of which is shown in Figure 5b. In this figure, the rows of coefficients are tangent to the inner circle (section of the inner cone in Figure 5a) confining the unexplored Fourier area. Each row of a corona comes from a different 2D FT and is identified by an azimuthal angle ϕ; the set of rows can obviously contain gaps corresponding to missing projections. These gaps can be filled as originally suggested in presenting SPARK, or in a different way (Lanzavecchia and Bellon, 1996). Let us assume, for the present discussion, that the set of projections is complete.

The complicated distribution of samples in Figure 5b can be divided into two propeller-like distributions, one of which is presented in Figure 5c. Either distribution contains a set of samples which are regularly spaced on the blades of a propeller and on concentric circles. Each point P within a corona can be identified by its coordinates (ϕ,ℓ), the azimuthal angle of the projection and its position on the semi-chord, as shown in Figure 5d. Since P is found on both propellers with different coordinates, two values of it can be independently recovered. This holds true for all points of the Cartesian grid enclosed within the corona, which are recovered in two copies. In the final reconstruction the two copies are eventually averaged; they can however be used to perform phase agreement tests (Frank *et al*., 1981) without dividing the set of projections into two groups, as is usually done with CBPM (Radermacher, 1988).

The shape of the 2D moving window used in conical tilt geometry is rather unusual as can be seen in the two examples of Figure 6. In most cases, the grid of samples used to reconstruct a point is enclosed within a mixed polygon formed by two straight segments and two arcs; points which are near the inner circle of the corona, however, are interpolated in a starry polygon obtained by prolonging to a small extent each blade on the opposite part of the chords. Blades are prolonged to maintain the interpolated point in the center of the moving window (Lanzavecchia and Bellon, 1996).

To obtain a quantitative evaluation of the performance of DFM in this geometry, we have formulated some phantoms made up of a number of Gaussian spheres; heights and half-height widths of the Gaussian profiles were assigned with random values. These phantoms were projected analytically and reconstructions were performed with SPARK and with our back-projection algorithm. The transforms recovered by SPARK and those computed from CBPM reconstructions were compared with the transforms of the original phantom, by considering the differences in moduli and phases of coefficients, with the obvious exclusion of those within the missing cone of the reconstructions. Table 2 shows the results, based on the following statistical indices (e.g., Giacovazzo, 1992):

$$R = \frac{\sum \| F_c | - k \bullet | F_o \|}{\sum | F_c |} \times 100$$

$$R' = \sqrt{\frac{\sum (| F_c | - k \bullet | F_o |)^2}{\sum | F_c |^2}} \times 100 \qquad (8)$$

$$R' = \sqrt{\frac{\sum (| F_c | - k \bullet | F_o |)^2}{\sum | F_c |^2}} \times 100$$

where F_c are the coefficients of the FT computed from the phantom and F_o are those recovered by the reconstruction. Phase agreement was tested with an index P, almost identical to the "Fourier ring phase residual" proposed by van Heel (1987):

$$P = \frac{\sum |F_c| \bullet |\Phi_c - \Phi_o|}{\sum |F_c|} \qquad (9)$$

where Φ_c and Φ_o, in radians, are the phase angles in original and in recovered Fourier coefficients.

Discussion and Concluding Remarks

Band-pass properties of MWSR

All interpolation algorithms behave as low-pass filters, with the exception of the complete Shannon reconstructions of functions which satisfy the conditions mentioned above. In the MWSR, the few samples enclosed within the window, usually from 6 to 16 depending upon the required accuracy, are regarded as a complete sampling interval. It is important to establish, for the small sampling interval, the maximum frequency transmitted without attenuation if all hypotheses under which the MWSR is adopted are verified. Though these conditions cannot generally be valid, the damping properties of interpolating kernels will suppress most aliasing errors. A MWSR is expected to attenuate, within the small sub-interval of the window, all frequencies higher than $M=(n-A-1)/2$, n being the window width and A the exponent of the cosine expression in Equation (5) (Lanzavecchia and Bellon, 1995). In theory, a kernel encompassing 16 samples with $A=3$ will attenuate all components higher than 6. For an entire sampling interval, the maximum frequency transmitted without attenuation is equal to MN/n, the latter term being the number of times the window is contained in the complete

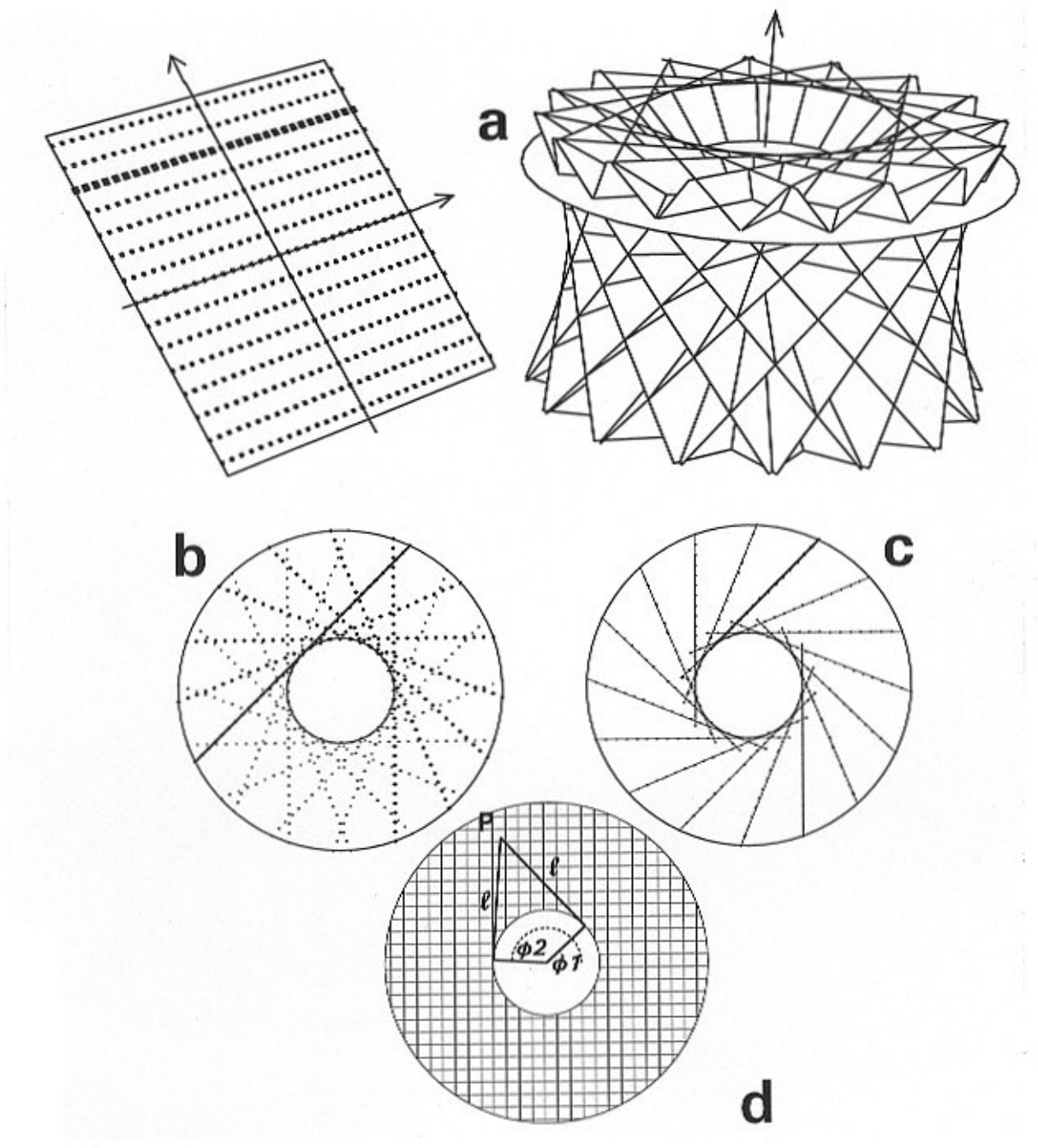

Figure 5. Conical tilt geometry in the Fourier domain: the resampling process. (**a**) Lay out of central sections in the 3D FT; a disk orthogonal to the cone axis cuts the sections. The central section at left (2D FT of a projection) shows the Cartesian array of discrete Fourier coefficients. The horizontal sampling rate is twice the vertical; this is obtained by appropriate padding of projections. The intersecting disk in (a) contains the annulus of samples shown in (**b**); the coefficients of central sections lie on chords of the outer circle, tangent to the inner one. (**c**) the system of chords is divided into two propeller-like sets of blades (only one is shown). Each propeller is regarded as a coordinate system (ℓ,ϕ) in which the experimental coefficients represent an equispaced set of samples. (**d**) a point P of the portion of Cartesian grid enclosed by the annulus is described by two sets of coordinates (ℓ,ϕ_1),(ℓ,ϕ_2), one for each set of blades.

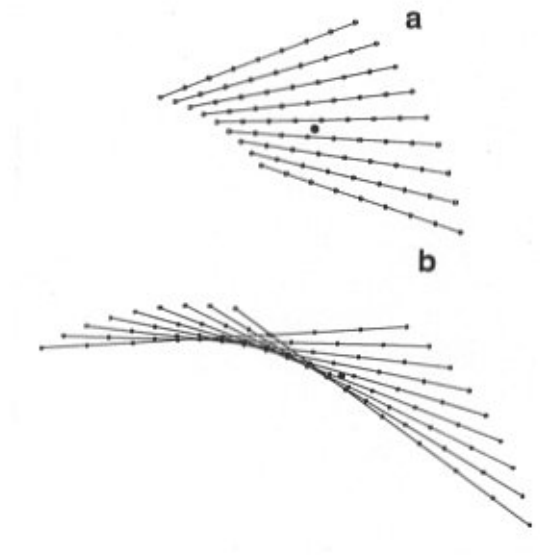

Figure 6. Different shapes of the 2D moving window in conical tilt geometry. The experimental samples on the annulus of Figure 5 are equally spaced in the (ℓ,ϕ) system, not so in an Euclidean metric. (a) if the point being resampled is internal to the annulus, the moving window has a convex shape. Near the inner border of the annulus, the blades are prolonged a bit, to maintain the point to be resampled in the center of the window which has the starry shape shown in (b).

interval (Lanzavecchia and Bellon, 1994). Thus, $\phi_{16}{}^{3}$, used in a 64-points interval is able, in theory, to pass unattenuated frequencies up to 24, or 75% the Nyquist frequency for this number of samples.

This band-pass criterion is quite useful in choosing the kernels appropriate for a particular task. Iterated resampling, for instance, is possible if one uses a kernel which transfers unattenuated components just beyond the maximum frequency present in the image. Since this maximum cannot be easily established, $\phi_{16}{}^{3}$ could be the appropriate choice. In X-ray CT, a function $\phi_{11}{}^{2}$ is adequate to reconstruct the high resolution images of Figure 4 whereas 3D electron tomographic reconstructions of phantoms and of real structures are done in our laboratory with function $\phi_{15}{}^{4}$. This accurate kernel is used "*ad abundantiam*" because the set of coefficients to be interpolated is fairly small (usually the reconstructed volume spans 64^3 voxels) if compared with that required in an X-ray CT reconstruction.

DFM vs. CBPM in electron tomography

Convoluted back-projection is a "robust" method to get reconstructions. Compared with DFM, its main advantage is that equispaced viewing angles are not required and gaps can be present, though projections need to be reasonably well distributed in space. Conversely, DFM needs angular directions evenly spaced and complete projection sets. However, a non regular distribution of projecting angles is amenable to a regular one with jitter errors. Moreover, angular gaps can be filled (Lanzavecchia and Bellon, 1996) by exploiting the nice properties of a set of projections ordered with regularly increasing azimuthal angles. This ordered set can be used to build up a 3D matrix in which the two fastest indices span the *x* and *y* axes of each projection and the third one spans the azimuthal axis in the interval [0, 2π). In the absence of noise and if there is a projection for each value of the azimuth, the 3D FT of the matrix is zero within an elliptic cone whose axis lies along the slower index. In the presence of noise, or if some plane of the matrix is zero because no projection is available at that angle, the elliptic cone will exhibit non-zero components which can be cancelled. Since the presence of signal in the cone implies a tomographic inconsistency of the ordered set, zeroing the cone means cancelling the part of noise which is not consistent with the projection process ("non tomographic noise", NTN). If some plane of the matrix is empty, then some information will appear on it upon inversion of the 3D transform. The process of zeroing the cone can be iterated a few times on a matrix containing the original projections plus what has appeared in the empty planes. The process is a kind of projection onto a convex set (POCS) sequence of iteration in which the target is represented by the Fourier transformed ordered set with the elliptic cone containing zero. Four or five iterations are usually enough to recover with good accuracy all missing projections (Lanzavecchia and Bellon, 1996).

It seems important to compare the intrinsic accuracy of CBPM and DFM, and this can be done in the conditions which make the DFM rigorously valid. We have done this comparison both for single axis and for conical tilt. A back-projecting program written for this purpose needs no weighting schemes to take into account arbitrary geometries or uneven distributions of projecting directions (Harauz and van Heel, 1986; Radermacher *et al.*, 1987). The ramp-filter shape was designed in real space to avoid the "dc-shift", an alteration of the mean value (Crawford, 1991). Since the filter convolution is performed in Fourier space, the performance of CBPM has also been tested with padding of projections to avoid artefacts arising from circular convolution (Rosenfeld and Kak, 1982).

Three-dimensional tomographic tests with single axis geometry were carried out with the same phantoms used to test DFM in conical tilt. Analytical projections of phantoms were computed for the interval [$-\pi/2$, $\pi/2$] to get a complete set of projections. Sets of this type might be obtained, even for entire organelles, on the high voltage EM (McEwen, 1992). The reconstructions by DFM were performed with the same program used with conical tilt geometry (the tilt angle θ being $\pi/2$). Four types of CBPM reconstructions

Table 2. Reliability indices *R*, *R′* and *P* obtained in reconstructions of phantom structures with convoluted back-projection (CBPM) and direct Fourier method (DFM) for conical tilt- and single axis tilt geometry. Methods adopted for CBPM are indicated in parentheses: LI is for linear interpolation and PD for padding used in the convolution; if MWSR is used in interpolation, the kernel is specified. Two types of data have been used in DFM reconstruction: projections separated by a regular amount $\Delta\phi$ (EQ) and, in conical tilt, projections whose angles are varied at random in the interval $\pm\Delta\phi/2$ (RND).

Algorithm	Conical tilt				Single axis tilt 360°		
	R	R′	P	time (s)	R	R′	P
CBPM (LI)	8.60	10.20	0.020	134	5.24	4.30	0.0122
CBPM (LI, PD)	7.50	10.10	0.016	153	3.50	1.96	0.0047
CBPM (φ_g^2)	6.50	10.10	0.018	313	3.13	3.89	0.0097
CBPM (φ_g^2, PD)	5.00	10.00	0.013	374	0.22	0.08	0.0010
DFM (EQ)	0.12	0.18	0.001	15	0.09	0.07	0.0007
DFM (RND)	3.05	2.06	0.012	15			

were carried out: with or without padding and with linear- or MWSR interpolation. The results, in terms of the indices R, R′ and P described above, are collected in Table 2. As one can see, our DFM yields high accuracy results and CBPM performs comparably provided that padding and MWSR are used. Thus, the equivalence of DFM and CBPM, which stand on a common theoretical ground, is rigorously verified in practice.

Table 2 reports also the comparison among the two methods for conical tilt (tilt angle $\theta=50°$). As can be seen, the fairly good agreement indices for CBPM reconstructions, obtained with padding and MWSR, are far from the extreme accuracy of DFM as implemented in SPARK. Though the phase index *P*, the most significant one, shows good agreement, the amplitudes of coefficients deviate appreciably from analytical values. The reason for this discrepancy is being investigated at present. Perhaps, the type of indices we are adopting are the most convenient for DFM; other indices, based on direct space (e.g., Herman, 1980), might yield more favorable results for CBPM.

Until now we have reported tests and agreement indices based on equispaced projections. One could argue that, with random conical tilt, errors will arise because the azimuthal angles are not rigorously equispaced (e.g., Frank, 1996). The effect of jittering azimuthal angles can be tested by computing analytical projections whose angles depart from equispaced ϕ values by random amounts in the range $\pm\Delta\phi/2$. If a DFM reconstruction is done by assuming jittering angles to be equispaced, the reliability indices obtained (see last line of Table 2) still look better than those obtained *via* CBPM with equispaced projections.

All tests illustrated till now are based on noise-free data; a problem still remains, concerning the behavior of the algorithms in the presence of noise. CBPM is a robust technique, and its widespread use in tomographic experiments confirms its reliability in different conditions as for the layout and the noise level of projections. DFM need special geometries and this limits its dissemination and the possibility of testing the algorithm in a number of situations. As for the type of experiments presented here, studies are in progress on noisy data sets of projections; preliminary results indicate that differences exist in the behavior of the two approaches; these differences tend to vanish if the consistency of noisy sets of projection is improved by filtering out non tomographic noise (Lanzavecchia and Bellon, 1996).

The opportunity offered by DFM in estimating accurate Fourier amplitudes on a Cartesian grid is quite useful in POCS applications. According to POCS theory (Sezan and Stark, 1984; Carazo and Carrascosa, 1987; Carazo, 1992), a set of constraints can be iteratively imposed on a reconstruction, to fill up the unexplored region of the Fourier transform. “Value” and “support” constraints are imposed in real space whereas the “measurement” constraint, to enforce the consistency of the POCS solution with known projections is usually imposed in the reciprocal domain (Frank, 1996). In single axis and conical tilt geometry, once the reconstruction has been constrained in real space, it is straightforward to impose the measurement constraint by

restoring, in its FT, the accurate samples obtained with DFM.

Compared to CBPM, DFM is a "flash" process. As mentioned above, this is true for DFM reconstructions of X-ray CT slices. For the 3D reconstructions of electron tomography, we can quote the times used by the two methods in reconstructing volumes of 64^3 voxels, with conical tilt geometry and 128 projections. On our workstation, DFM requires 15 seconds and CBPM, with padding and MWSR, 350 seconds. These data show that the reconstruction step with either methods is not as time consuming as other tasks encountered in electron tomography, such as the orientation of large sets of images, their classification with multi-variate statistical analysis and the final restoration with POCS techniques. The fact that a DFM reconstruction is obtained in a few seconds is, anyhow, a nice aspect of the approach.

Concluding remarks

We have illustrated above the outstanding behavior of the moving window Shannon reconstruction in a number of applications in real and Fourier domain. Its extensive use for quite a few years (Bellon and Lanzavecchia, 1990) has allowed us to gain a wide experience with it and to embed it in a variety of different algorithms used in electron microscopy (e.g., Lanzavecchia *et al*., 1994).

The most interesting applications of this interpolation is the accurate resampling required to convert one coordinate system to another in Fourier domain. This possibility might be important in other applications, different from the problems of tomographic reconstruction, which could be devised to cope with other problems. In this connection, a fast DFM to obtain 2D and 3D Radon transforms is in progress in our laboratory and the use of the MWSR is being exploited in the Radon domain. The possibility to resample accurately a function in different domains and in different coordinate systems is, potentially, of a much wider use that we can foresee at present.

Acknowledgements

This work has been financially supported by the Italian Ministry for University and Research (40% and 60%), and by the National Research Council of Italy. The authors wish to thank Siemens AG of Erlangen for the raw data used in the reconstructions of Figure 4 and S. and S. Tamm of the Marine Biological Institute of Woods Hole for micrographs of which the spectra are shown in Figure 3.

References

Bellon PL, Lanzavecchia S (1990) POLCA, a library running in a modern environment, implements a protocol for averaging randomly oriented images. Comp Appl Biosci **6**: 271-277.

Bellon PL, Lanzavecchia S (1992) Pattern reconstruction in ultrastructural morphology. J Microsc **168**: 33-45.

Bellon PL, Lanzavecchia S (1995) A direct Fourier method (DFM) for X-ray tomographic reconstructions and the accurate simulation of sinograms. Int J Biomed Comput **38**: 55-69.

Bellon PL, Lanzavecchia S (1997) Fast direct Fourier methods, based on 1- and 2-pass coordinates transformation, yields accurate reconstructions of X-ray CT clinical images. Physics Medicine Biol **42**: 443-463.

Brigham OE (1974) The Fast Fourier Transform. Prentice-Hall, Englewood Cliffs, NJ. pp 99-102.

Carazo JM, Carrascosa JL (1987) Information recovery in missing angular cases: an approach by convex projections method in three dimensions. J Microsc **145**: 23-43.

Carazo JM (1992) The fidelity of 3D reconstructions from incomplete data and the use of restoration methods. In: Electron Tomography. Frank J (ed). Plenum Press, New York. pp 117-164.

Clark JJ, Palmer MR, Lawrence PD (1985) A transformation method for the reconstruction of functions from nonuniformly spaced samples. IEEE Trans Acoust Speech Signal Processing **33**: 1151-1165.

Crawford CR (1991) CT filtration aliasing artifacts. IEEE Trans Med Imaging **10**: 99-102.

Crowther RA, Sleytr UB (1977) An analysis of the fine structure of the surface layers from two strains of *Clostridia*, including correction for distorted images. J Ultrastruct Res **58**: 41-49.

Frank J (1996) Three-Dimensional Electron Microscopy of Macromolecular Assemblies. Academic Press, New York. pp 182-143.

Frank J, Verschoor A, Boublik M (1981) Computer averaging of electron micrographs of 40S ribosomal subunits. Science **214**: 1353.

Giacovazzo C (1992) Fundamentals of Crystallography. International Union of Crystallography, Oxford University Press. pp 320-321.

Harauz G, van Heel M (1986) Exact filters for general geometry three dimensional reconstruction. Optik **73**: 146-156.

Henderson R, Baldwin JM, Downing KH, Lepault J, Zemlin F (1986) Structure of purple membrane from *Halobacterium halobium*: recording, measurement and evaluation of electron micrographs at 3.5 Å resolution. Ultramicroscopy **19**: 147-178.

Henderson R, Baldwin JM, Ceska TA, Zemlin F, Beckmann E, Downing KH (1990) Model for the structure of bacteriorhodopsin based on high-resolution electron cryomicroscopy. J Mol Biol **213**: 899-929.

Herman GT (1980) Image Reconstruction from

Projection: The Fundamental of Computerized Tomography. Academic Press, New York. pp 137-141.

Hoppe W, Hegerl R (1980) Three-dimensional structure determination by electron microscopy (non-periodic specimens). In: Computer Processing of Electron Microscope Images. Hawkes PW (ed). Springer-Verlag, Berlin, pp. 127-185.

Hou HS, Andrews HC (1978) Cubic splines for image interpolation and digital filtering. IEEE Trans Acoust, Speech, Signal Processing. **26**: 508-517.

Jap BK, Walian PJ, Gehring K (1991) Structural architecture of an outer membrane channel as determined by electron crystallography. Nature **350**: 167-170.

Lanzavecchia S, Bellon PL (1994) A moving window Shannon reconstruction for image interpolation. J Visual Comm Image Repres **5**: 255-264.

Lanzavecchia S, Bellon PL (1995) A bevy of novel interpolating kernel for the Shannon reconstruction of high band pass images. J Visual Comm Image Repres **6** 122-131.

Lanzavecchia S, Bellon PL (1996) Electron tomography in conical tilt geometry: the accuracy of a direct Fourier method (DFM) and the suppression of non tomographic noise. Ultramicroscopy **63**: 247-261.

Lanzavecchia S, Dallai R, Bellon PL, Afzelius BA (1991) The sperm tail of a Gall Midge and its microtubular arrangement studied by two strategies of image analysis (Cecidomyiidae, Diptera, Insecta). J Struct Biol **107**: 65-75.

Lanzavecchia S, Bellon PL, Scatturin V (1993) SPARK, a kernel of software programs for spatial reconstruction in electron microscopy. J Microsc **171**: 255-266.

Lanzavecchia S, Bellon PL, Dallai R, Afzelius BA (1994) Three dimensional reconstructions of accessory tubules observed in the sperm axonemes of two insect species. J Struct Biol **113**: 225-237.

Lewitt RM (1983) Reconstruction algorithms: transform methods. Proc IEEE **71**: 390-408.

Matej S, Bajla I (1990) A high-speed reconstruction from projections using direct Fourier method with optimized parameters. An experimental analysis. IEEE Trans Med Imaging **9**: 421-429.

McEwen BF (1992) Three-dimensional reconstructions of organelles and cellular processes. In: Electron Tomography. Frank J (ed). Plenum Press, New York. pp 281-311.

Papoulis A (1962) The Fourier Integral and its Applications. McGraw-Hill, New York. pp 42-47.

Papoulis A (1966) Error analysis in sampling theory. Proc IEEE **54**: 947-955.

Peng H, Stark H (1987) Direct Fourier reconstruction in fan-beam tomography. IEEE Trans Med Imaging **6**: 209-219.

Radermacher M, Wagenknecht T, Verschoor A, Frank J (1987) Three-dimensional reconstruction from a single exposure, random conical tilt series, applied to the 50S ribosomal subunit of *Escherichia coli*. J Microsc **146**: 113-136.

Radermacher M (1988) Three-dimensional reconstruction of single particles from random and nonrandom tilt series. J Electron Microsc Techn **9**: 359-394.

Rosenfeld A, Kak AC (1982) Digital Picture Processing. Academic Press, New York. pp 353-430.

Rudin W (1974) Real and Complex Analysis. McGraw-Hill, New York. pp 200-202.

Saxton WO, Dürr R, Baumeister W (1992) From lattice distortion to molecular distortion: characterising and exploiting crystal deformation. Ultramicroscopy **46**: 287-306.

Sezan MI, Stark H (1984) Tomographic image reconstruction from incomplete view data by convex projections and direct Fourier inversion. IEEE Trans Med Imaging **3**: 91-98.

Shannon CE (1949) Communication in the presence of noise. Proc IRE **37**: 10-21.

Stark H, Woods JW, Paul I, Hingorani R (1981) An investigation of computerized tomography by direct Fourier inversion and optimum interpolation IEEE Trans Biomed Eng **28**: 496-505.

Tosoni L, Lanzavecchia S, Bellon PL (1995) Surface rendering in electron tomography: a heuristic approach. J Microsc **179** 306-313.

Unser M, Thévenaz P, Yaroslavsky L (1995) Convolution-based interpolation for fast, high-quality rotation of images. IEEE Trans Image Processing **4**: 1371-1381.

Van Heel M (1987) Similarity measures between images. Ultramicroscopy **21** 95-100.

Wolberg G (1990) Digital Image Warping. IEEE Computer Society Press, Los Alamitos, CA. pp 95-116.

Yuen CK, Fraser D (1979) Digital Spectral Analysis. CSIRO Pitman, Adelaide. pp 14-16.

Discussion with Reviewers

M. Radermacher: How does the algorithm perform, as compared to others, when the angular sampling is incomplete, i.e., some projections are missing?

Authors: For a DFM based on MWSR, the set of evenly space projections must be complete; if gaps exist then they must be filled, as briefly reported above, with use of the strategy proposed elsewhere (Lanzavecchia and Bellon, 1996). In that paper, we show that even when as many as 25% of projections are missing, and noise is present, the quality of the reconstruction does not change significantly with respect to that obtained from a complete set. However, our experience with CBPM applied to uneven distribution of projections and with the related weighting schemes is

still limited; studies are in progress to compare the results of reconstructions from incomplete sets and from sets in which missing projections have been recovered.

For the problem of uneven sampling, a strategy we are planning to explore consists of a mixed interpolation scheme based on MWSR and splines, since it is commonly assumed that, in tomographic experiments, resampling the angular direction is less critical than the radial one (Matej and Bajla, 1990). In other words, it is possible to design an interpolation technique with MWSR in the radial direction and with splines in the angular one. Cubic splines do not need equally spaced data, so that gaps can simply be regarded as regions of uneven sampling.

N. Bonnet: The problem of uneven sampling of the projections in tomographic reconstruction has been tackled by several authors including M. van Heel, M. Radermacher (your references) and Boisset *et al*. (these proceedings). Do you believe your interpolation method is also able to cope with this problem and how does it compare with the previous approaches (adapted filters and topological selection)?

Authors: Our DFM approach in electron tomography is limited until now to single axis and conical tilt geometries; a bit of randomness can be managed as we point out in answering to the question of M. Radermacher. For completely random orientations of the projections, a resampling scheme to obtain the Fourier transform in Cartesian coordinates needs still be devised, though some ideas are flying around in our lab (see comments to the previous question). Adapted filters and algebraic reconstructions seem, at the moment, the only way to cope with the problem. A topological selection of projections may be useful for simpler and faster reconstruction algorithms, although a proper weighting scheme would allow algebraic reconstruction to take advantage of the information coming from the entire set of available images.

A DFM implementation of the reconstruction from random projections would possess the advantage of eliminating all approximations related to the choice of weighting functions, which is somewhat arbitrary. The slightly different weighting schemes proposed by Radermacher (1988) and Harautz and van Heel (1986) limit the support of the selected weighting function in reciprocal space in order to speed up computations. Probably, these approximations are good enough for the level of noise in the micrographs and for the quality of the results expected.

A resampling scheme for a DFM with completely random orientations might be feasible in the future, by taking advantage of a 3D Radon inversion whose back-projection implementation has been proposed by M. Radermacher (these proceedings).

N. Bonnet: In your paper, you claim that many image processing techniques require to perform "sophisticated" interpolation rather then the "usual" linear or spline interpolations. The advantage of your interpolation scheme is demonstrated theoretically (study of transfer functions) in Figure 2. Could you indicate some general figure of merit for the importance of the improvement you expect in practical situations? For instance, could you give the equivalent of Figure 4 when linear interpolation is used for the direct Fourier reconstruction, instead of MWSR.

Authors: Since the advent of X-ray CT, back-projection algorithms have always been preferred to DFM, though the latter technique was universally thought to be faster. The reason is due to a number of artefacts in the reconstructions such as rings, cambers and cross-shaped ripples, which often appear in DFM images (e.g., Magnusson, 1993). These artefacts are mostly caused by the poor performance of linear interpolation in resampling very strong coefficients, i.e., the low frequency components. In the image presented in Figure 4, artefacts introduced by linear interpolation would not be evident since the wide dynamic range of the reconstruction is compressed into 256 gray levels; this compression is adopted as a standard in clinical examinations of inner ear bones. Quite a different situation is encountered in examining brain soft tissues. In these reconstructions the radiologist's attention is focused on about 3-5% of the dynamic range, within which tiny differences of contrast play a fundamental role in the diagnosis. An image of this type, a head slice studied for possible brain problems, is shown in Figure 7. The two reconstructions shown there have been obtained with MWSR (Fig. 7a) and linear interpolation (Fig. 7b). The strong artefacts of linear interpolation clearly make the reconstruction in Figure 7b nonsensical.

J.M. Carazo: Your point about the possibility of using two estimations of each Fourier transform sample for resolution assessment is quite interesting, could you elaborate on it further? How would it compare with the usual *a priori* splitting of the projections?

Authors: A set of projections in conical tilt geometry contains redundant information; this is evident in Figure 5 if one considers how the 2D transform planes intersect one another. With noisy data, this redundancy is useful for averaging the information and obtaining an improvement of the signal to noise ratio; this is true for both DFM and CBPM. In our DFM, this redundancy is exploited to perform two independent resamplings of each point of the Cartesian transform. Since each set of resampled coefficients yields an independent reconstruction, the two reconstructed maps can be compared to assess the resolution limit. In principle, this is perfectly equivalent to an *a priori* split of projections into two sets which are used in two independent

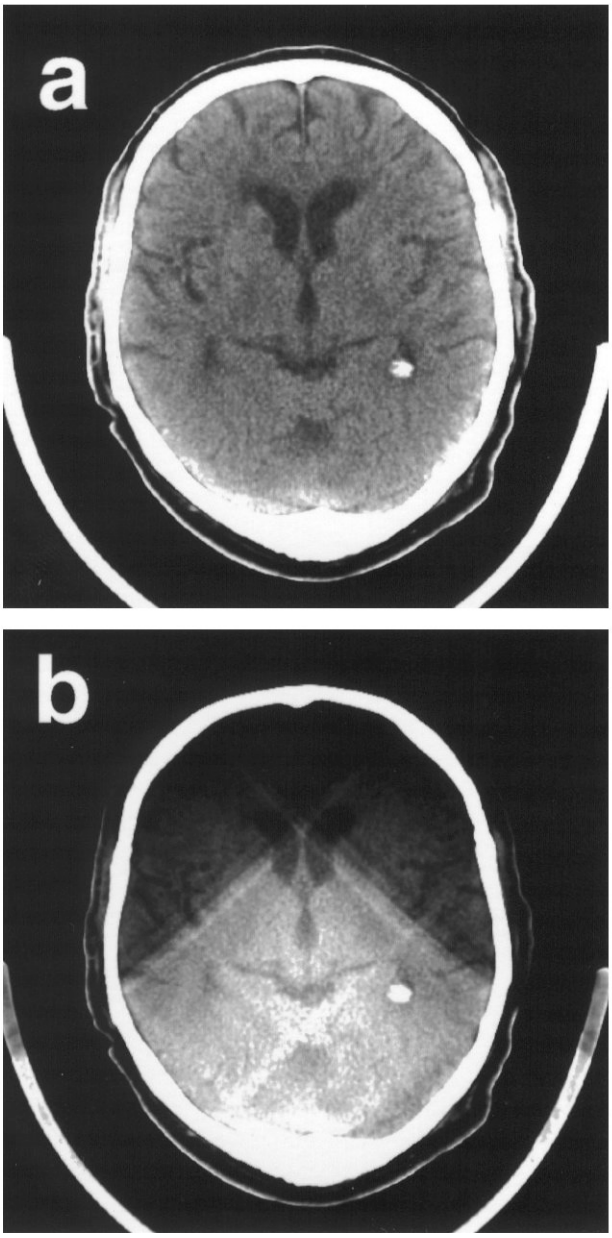

Figure 7. X ray CT reconstruction of a head section. Only about 3% of the total dynamic range is shown in the 256 grey level of the representation, as required in clinical diagnostics. This range is selected to highlight the contrast within the brain tissue. Both images have been obtained by DFM reconstruction. (**a**) Reconstruction obtained with MWSR algorithm. (**b**) Reconstruction obtained with linear interpolation. The strong artefacts in (b) make this image completely useless.

reconstructions. The two strategies are equivalent if the errors of the reconstruction processes are not taken into account. Actually, the splitting of data lowers the sampling rate in the angular direction of reciprocal space. With DFM, this means that the probability of gaps increases and that the quality of interpolation may be worse. With CBPM, the lowered sampling rate implies a weighting scheme far from the analytic one, which requires equally spaced projections. On the basis of the criterion that links the resolution to the number of projections (Radermacher, 1988), it is clear that reconstructions obtained from split data are expected to be poorer, unless the number of available images is very high. In contrast, the two reconstructions coming from the independent resampling of a unique set of projections behave, with respect to the resolution criterion, as the reconstruction from the full set does.

Additional Reference

Magnusson M (1993) Linogram and other direct Fourier methods for tomographic reconstruction. Doctoral Thesis, Linköping Studies in Science and Technology. Dissertation No 320. University of Linköping, Sweden. pp 153-186.